LETTER

doi:10.1038/nature22052

Observed quantization of anyonic heat flow

Mitali Banerjee[1], Moty Heiblum[1], Amir Rosenblatt[1], Yuval Oreg[1], Dima E. Feldman[2], Ady Stern[1] & Vladimir Umansky[1]

The quantum of thermal conductance of ballistic (collisionless) one-dimensional channels is a unique fundamental constant[1]. Although the quantization of the electrical conductance of one-dimensional ballistic conductors has long been experimentally established[2], demonstrating the quantization of thermal conductance has been challenging as it necessitated an accurate measurement of very small temperature increase. It has been accomplished for weakly interacting systems of phonons[3,4], photons[5] and electronic Fermi liquids[6–8]; however, it should theoretically also hold in strongly interacting systems, such as those in which the fractional quantum Hall effect is observed. This effect describes the fractionalization of electrons into anyons and chargeless quasiparticles, which in some cases can be Majorana fermions[2]. Because the bulk is incompressible in the fractional quantum Hall regime, it is not expected to contribute substantially to the thermal conductance, which is instead determined by chiral, one-dimensional edge modes. The thermal conductance thus reflects the topological properties of the fractional quantum Hall electronic system, to which measurements of the electrical conductance give no access[9–12]. Here we report measurements of thermal conductance in particle-like (Laughlin–Jain series) states and the more complex (and less studied) hole-like states in a high-mobility two-dimensional electron gas in GaAs–AlGaAs heterostructures. Hole-like states, which have fractional Landau-level fillings of 1/2 to 1, support downstream charged modes as well as upstream neutral modes[13], and are expected to have a thermal conductance that is determined by the net chirality of all of their downstream and upstream edge modes. Our results establish the universality of the quantization of thermal conductance for fractionally charged and neutral modes. Measurements of anyonic heat flow provide access to information that is not easily accessible from measurements of conductance.

The fractional quantum Hall state, first observed in 1982, still provides a spectrum of challenges. The universal quantized electrical Hall conductance G_H, with current I flowing in downstream, chiral, one-dimensional edge modes, is directly related to the filling ν of Landau levels in the bulk: $G_H = dI/dV = \nu G_0$, with V the voltage, $G_0 = e^2/h$ the quantum of electrical conductance, e the elementary charge and h the Planck constant. The nature and number of the edge modes are not dictated by topological considerations and may take different values for different fractional quantum Hall states at the same Landau-level filling[9,10]. Consequently, the electrical conductance reflects the number and conductance of downstream charged chiral modes, but is independent of the total number of modes, their chirality and their character.

The thermal conductance $g_Q = dJ_Q/dT$, with J_Q the heat current and T the temperature, was studied for a single heat-conducting channel first by John Pendry in 1983[1], who set an upper bound on the thermal conductance of $g_Q = \kappa_0 T$, with $\kappa_0 = \pi^2 k_B^2/(3h)$ and k_B the Boltzmann constant. For edge states of Abelian quantum Hall states, both integer and fractional, Kane and Fisher[10] showed that the thermal conductance is closely related to the net number of edge modes: $g_Q = N_{net}\kappa_0 T$, with $N_{net} = N_d - N_u$ defined as the difference between the numbers of downstream and upstream edge modes[10].

Here we extend previous studies of thermal transport[3–8] to a strongly interacting system provided by the fractional quantum Hall effect[2]. Our aim is to test the notion that the quantum of thermal conductance is universal and therefore independent of the charge of the quasiparticles. Specifically, we first establish our method by studying non-interacting electrons ($\nu = 1$ and $\nu = 2$). We then extend the study to the particle-like $\nu = 1/3$ Laughlin state, with electrical conductance $G_H = (1/3)G_0$ and quasiparticle charge $e^* = e/3$, which is expected to have one unit of the thermal quantum conductance ($g_Q = 1\kappa_0 T$, without the factor of 1/3). Finally, we study the intriguing and complex hole-like states $\nu = 2/3$, 3/5 and 4/7, in which case the fractional quantum Hall liquid also supports upstream chiral edge modes[13]; for example, the standard picture of the $\nu = 2/3$ state is a downstream charge mode with electrical conductance $G_H = (2/3)G_0$ and an upstream chargeless (neutral) mode[9,10,13–16]. In general, these topological modes might be augmented by extra pairs of counter-propagating modes if the confining potential is soft and if edge reconstruction is established[16]. For $\nu = 2/3$, because $N_{net} = 0$ the heat flow must be fully diffusive and so the net thermal conductance should approach zero for increasing system size[10]. For the other hole-like states

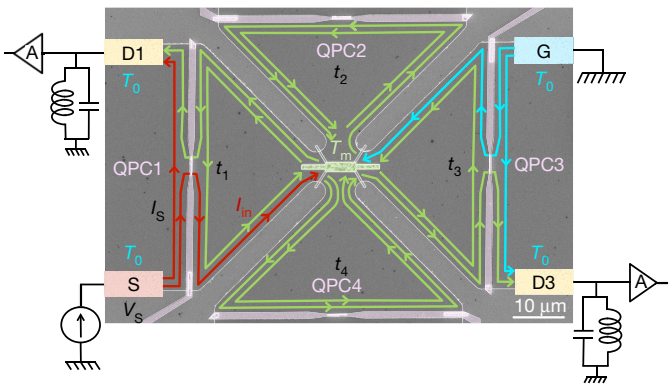

Figure 1 | Configuration of the device. The device is fabricated in a high-mobility two-dimensional electron gas embedded in a GaAs–AlGaAs heterostructure. An SEM micrograph of the four-armed device, which has a small floating ohmic contact at its centre (green; the depleting groves underneath are not visible) and a quantum point contact (QPC) in each arm (an air bridge shorts the two sides of the split-gate of the QPC). The source (S), drain (D1 and D3) and ground (G) contacts are drawn not to scale. In this example, $\nu = 2$ and QPC2 and QPC4 are fully pinched ($M \equiv N = 2$), while QPC1 and QPC3 transmit only the outmost edge mode and fully reflect the inner mode (t_i is the transmission coefficient of QPC$_i$). The source current (I_S, red) impinges on QPC1, which transmits a current I_{in} (here $I_{in} = I_S/2$), which is absorbed in the floating contact. Edge modes (green) at potential V_m and temperature T_m move from the floating contact into the four arms (in arms 2 and 4 they are fully reflected). Cold edge modes, at temperature T_0 (blue) arrive from the grounded contacts. A resonant (LC) circuit at each drain, with centre frequency $f_0 = 695$ kHz and bandwidth $\Delta f = 10$–30 kHz, depending on ν, filters the signal, which is amplified by the voltage pre-amplifier (cooled to 4.2 K) and then by a room-temperature amplifier (total gain is about 1,000). The amplified signal is measured by a spectrum analyser with similar f_0 and Δf.

[1]Braun Center for Sub-Micron Research, Department of Condensed Matter Physics, Weizmann Institute of Science, Rehovot 76100, Israel. [2]Department of Physics, Brown University, Providence, Rhode Island 02912, USA.

studied, $\nu = 3/5$ and $\nu = 4/7$, the net heat current is expected to propagate in the upstream direction[10,12].

Our experimental set-up is based on the core idea put forward in ref. 8, wherein the thermal conductance in the integer quantum Hall regime was measured. However, here we exploit a more flexible implementation: a scanning electron microscopy (SEM) image of the 'heart' of the four-armed structure is shown in Fig. 1 (for a full description of the device, see Extended Data Fig. 1). A DC input power is provided by a source voltage V_S and driving current $I_S = G_H V_S$, with propagating power $P_S = 0.5 I_S V_S$. The current impinges on a floating reservoir, $I_{in} = t_1 I_S$, where $t_1 = \nu_{QPC1}/\nu$ is the transmission coefficient of quantum point contact 1 (QPC1), ν_{QPC1} is its Landau-level filling and ν is the filling of the system as a whole. The outgoing current from the floating reservoir splits into M arms ($M = 2$, 3 or 4, as determined by the QPCs in the arms; equal splitting of the current into the open arms is demonstrated in Extended Data Fig. 2), carrying power $P_{out} = P_{in}/N$, where N is the number of outgoing current-carrying modes, with the dissipated power in the reservoir given by $\Delta P = P_{in} - P_{out} = 0.5 I_{in} V_S (1 - N^{-1})$. The reservoir reaches a new thermal equilibrium at temperature T_m, at which point the dissipated power is equal to the sum of the power carried by phonons (to the bulk) and that of the chiral edge modes: $\Delta P = \Delta P_{ph} + \Delta P_e$. If universality is established, then $\Delta P_e = 0.5 N \kappa_0 (T_m^2 - T_0^2)$, where T_0 is the electron base temperature; the heat carried by the phonons is expected to obey $\Delta P_{ph} = \beta (T_m^5 - T_0^5)$, where β is a constant that depends on the size of the heated reservoir[17]. The heat carried by the phonons is negligible in comparison to the electronic contribution for $T_m < 35$ mK (ref. 17). The temperature T_m is determined from thermal noise measurements in one or two of the arms (see Methods).

Deducing the thermal conductance with a reasonable accuracy necessitates a careful determination of the parameters of the system. A few important considerations are: (i) the gain of the amplification chain must be accurately determined (see Methods); (ii) unavoidable reflections from the floating small contact should be minimized (found to be <2%, with negligible contribution to undesirable shot noise); (iii) excess noise produced by the source contact should be negligible (or otherwise must be subtracted); (iv) the outgoing current must split equally between all of the conducting arms; (v) full charge and temperature equilibration was assumed to take place in the floating contact (charging of the floating contact is negligible due to the very short charging (RC) time)[8]; and (vi) heat flow via phonons is independent of the number of conducting arms, and depends only on the temperature T_m. We address issues concerning propagation length and energy flow through the bulk later.

First we elaborate on measurements at $\nu = 2$, at which two edge modes leave the source and QPC1 determines the number of modes that impinge on the floating contact. The excess thermal noise S_{th} was measured as a function of I_{in} for a few different filling factors of the QPCs in the arms, ν_{QPCi} (Fig. 2a). The temperature T_m, determined from the thermal noise (see Methods), is plotted as a function of the dissipated power ΔP in Fig. 2b (in this case $T_0 = 30$ mK). Because the temperature of the electrons was relatively high in these measurements, the phonon contribution was subtracted (as demonstrated in Fig. 2c): $\delta P = \Delta P(N_i, T_m) - \Delta P(N_j, T_m)$, with N_i and N_j the total number of outgoing modes from the central floating contact for different QPC settings. The normalized coefficient of the dissipated power, defined as $\lambda = \delta P/(\kappa_0/2)$, is plotted for six different configurations of $\Delta N = N_i - N_j$ in Fig. 2c. The average thermal conductance of a single electronic mode was found to be $g_Q = (0.98 \pm 0.03)\kappa_0 T$ (where here and henceforth $T = (T_0 + T_m)/2$ and the specified error is the standard deviation), in an excellent agreement with the expected quantization (Fig. 2c, inset). We also find the phonon coefficient β for the floating contact, $\beta \approx 3$–5 nW K^{-5}. Similar measurements were also performed for $\nu = 1$, for which there are fewer configurations (because there is one charge mode in each arm). Here, the average thermal conductance per one-dimensional mode was $g_Q = (0.9 \pm 0.1)\kappa_0 T$ (see Extended Data Fig. 3). Note that the error specified for g_Q was calculated from only the randomly scattered data; systematic errors (if they exist) were neglected (see Methods).

We now describe measurements for the most prominent fractional state, $\nu = 1/3$. Because this state is the first filled Landau level of composite fermions ($\nu_{CF} = 1$), with electronic filling $\nu = \nu_{CF}/(2\nu_{CF} + 1)$

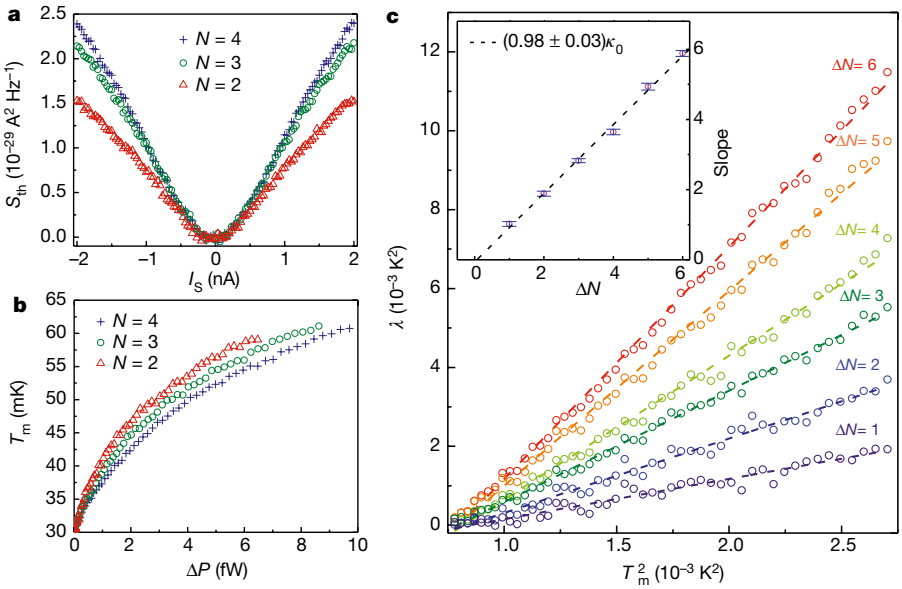

Figure 2 | Measurements in the integer quantum Hall regime at filling $\nu = 2$. **a**, Excess thermal noise S_{th} plotted as a function of the source current I_S in three different configurations ($N = 2$, 3 and 4), wherein only the outmost mode is transmitted through the QPCs. $T_0 = 30$ mK. **b**, The calculated temperature of the floating contact T_m plotted as a function of the dissipated power ΔP in the three configurations. **c**, Subtracting the dissipated power at T_m for different N (where N is the total number of outgoing current-carrying modes) eliminates the contribution of the phonons. We plot $\lambda = \delta P/(\kappa_0/2)$, with $\delta P = \Delta P(N_i, T_m) - \Delta P(N_j, T_m)$, as function of T_m^2 for six combinations of N_i and N_j (six different $\Delta N = N_i - N_j$). The open circles are the data and the dashed lines are linear least-square fits. Inset, the slopes ($g_Q \Delta N$) of the linear fits for each of the six combinations (open circles; error bars, standard deviation). A linear fit (dashed black line) to these slopes reveals an average thermal conductance of $g_Q = (0.98 \pm 0.03)\kappa_0 T$ for each one-dimensional mode.

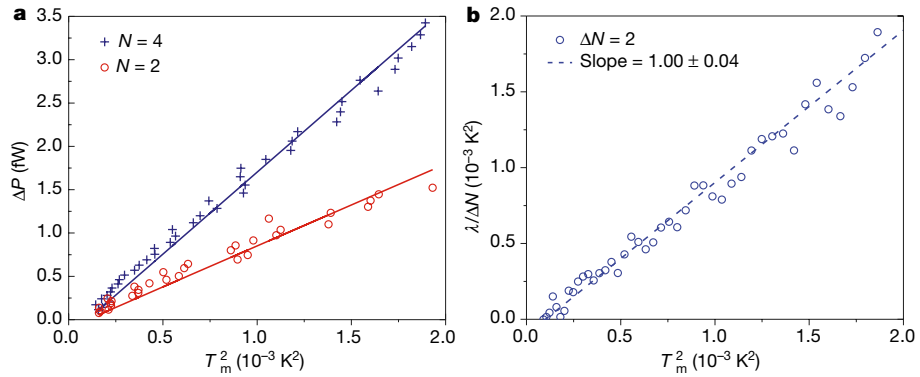

Figure 3 | Measurements in the fractional quantum Hall regime at filling $\nu = 1/3$. a, Total power ΔP carried out by the fractional edge modes from the floating contact for two different configurations ($N = 4$, blue; $N = 2$ red). The theoretical expectations $\Delta P_e = 0.5N\kappa_0 T_m^2$ (with no phonon contribution in this temperature range) for the two cases are shown as solid lines. The root-mean-square of the data points deviates from the expected values by 4% for $N = 4$ and 2% for $N = 2$. $T_0 = 10$ mK. **b**, A plot of $\lambda/\Delta N = \delta P/(\kappa_0/2)/\Delta N$, with $\delta P = \Delta P(N_i = 4, T_m) - \Delta P(N_j = 2, T_m)$, so any phonon contribution is subtracted, as a function of T_m^2. A linear fit (dashed line) to the data gives $g_Q = (1.00 \pm 0.045)\kappa_0 T$.

(ref. 18), it harbours a single chiral downstream edge mode. (This is expected when the edge potential is sharp; for a soft edge potential, edge reconstruction may add pairs of counter-propagating modes, but these should not affect the thermal conductance[16,19].) Consequently, the thermal conductance of this state is expected to be $g_Q = 1\kappa_0 T$—the same as that of the $\nu = 1$ state. We studied this state in the lower-density sample (see Methods), which has a larger floating contact (the measured reflection coefficient from that contact was about 2%). With a lower electron temperature, $T_0 \approx 10$ mK, the power dissipation was kept small, thus avoiding a large increase in T_m and enabling us to neglect the contribution of the phonons altogether. Source noise (on top of the direct current), multiplied by a factor of $N^{-2} = M^{-2}$ (here and henceforth, because each arm has one charge mode, $N \equiv M$), was subtracted from the measured thermal noise. Because both the electrical conductance (G_H) and temperature range (T_m) were small, the excess thermal noise was small, thereby necessitating a long averaging time.

The dissipated power as a function of T_m^2 is plotted in Fig. 3a for two configurations, $N = 4$ and $N = 2$, along with the theoretically expected dependence for $g_Q = 1\kappa_0 T$. The absence of a T_m^5-dependent term in δP is verification that the phonon contribution is negligible. In Fig. 3b we plot λ for $\Delta N = N_i - N_j = 4 - 2 = 2$ as a function of T_m^2, to confirm that the phonon contribution is completely eliminated. The average thermal conductance is found to be $g_Q = (1.0 \pm 0.04)\kappa_0 T$, once again in excellent agreement with expectations.

The hole-like states in the first Landau level, with fractional fillings $1/2 < \nu < 1$, belong to the same composite-fermion hierarchy as the particle-like states. (However, the residual magnetic field that remains after flux attachment of two flux quanta is opposite in direction to the original field and so edge modes propagate in both chiralities.) The composite-fermion filling in these states is related to the actual electron fractional filling via $\nu = \nu_{CF}/(2\nu_{CF} - 1)$. We studied the states $\nu = 2/3$, $\nu = 3/5$ and $\nu = 4/7$, which have theoretically predicted thermal conductances of $g_Q = 0$, $g_Q = -1\kappa_0 T$ and $g_Q = -2\kappa_0 T$, respectively. Astonishingly, for $\nu = 3/5$ and 4/7, heat is expected to propagate in the opposite direction to that of the charge current (hence the negative signs)[10,12]; however, the actual sign of the net chirality could not be determined with our device configuration.

In our experiment, excited downstream modes leave the floating contact, but retain an electrochemical potential and temperature T_m equal to those of the floating contact, and propagate along one edge of each arm, while excited upstream neutral modes, also heated to T_m, emanate from the opposite side of the contact and propagate along the other edge of the arm. Charge and neutral modes arrive back from the grounded contacts (which are at T_0; blue lines in Fig. 1), intermix and equilibrate with the hotter downstream modes, thereby returning energy to the floating contact. The initial ballistic propagation of downstream modes undergoes an inter-edge scattering at long enough propagation length, and heat dissipation via the edge modes is restricted.

To understand the difference between the quantization of the thermal conductance at $\nu = 2/3$ and at other filling factors, we consider a simplified model of thermal transport on an edge of a quantum Hall state with one downstream mode ($N_d = 1$) and N_u upstream modes, with $N_u = 1$ (see below) at $\nu = 2/3$, $N_u = 2$ at $\nu = 3/5$ and $N_u = 3$ at $\nu = 4/7$. Using conservation of energy and adopting Newton's law of cooling for thermal relaxation between counter-propagating modes on the same edge, we obtain a linear system of differential equations that describes the heat flow in this system (see equations (4)–(7) in Methods). We find that for $N_u > N_d$ the temperature of the modes converges to that of the upstream modes. The temperature difference between the downstream mode and the upstream modes vanishes as a decaying exponential function of the distance from the floating contact (with a relaxation length ξ). When the size of the system is much larger than the relaxation length ($L \gg \xi$), the heat is carried along one edge of each arm and the quantization should be precise. In contrast, for $N_u = N_d$ (as is the case for $\nu = 2/3$), the temperatures of the modes depend only linearly on the distance from the contacts, and the temperature difference between the downstream and upstream modes remains constant along the edge for a certain length of each arm. Consequently, the thermal conductance approaches zero only linearly in $1/L$: $g_Q = 2\kappa_0 T^2/(1 + L/\xi)$. Furthermore, because this is true for both edges, heat flows equally along both edges of each arm.

We measured the thermal noise in these three hole-like states. The total dissipated power (including phonons) for $N = 4$ is plotted as function of T_m^2 in Fig. 4a, along with the theoretically expected values. The normalized power λ, for $\Delta N = N_i - N_j = 4 - 2 = 2$, is plotted as function of T_m^2 in Fig. 4b.

The state with $\nu_{CF} = 2$ or $\nu = 2/3$ is expected to support an equal number of downstream and upstream modes[9,10]. Our current understanding is that there are two downstream modes, each with conductance $G_0/3$, and two upstream modes, which are neutral[19–21]. The partitioned charge in a partly pinched QPC (for example, for $\nu_{QPC} = 1/3$) has previously been measured via shot noise[21] and has been verified to be $e^* = 2e/3$ (see Extended Data Fig. 4 for the thermal noise and Extended Data Fig. 5 for the shot noise).

The total out-flowing electronic power ΔP for $M = N = 4$ is plotted as function of T_m^2 in Fig. 4a ($\nu = 2/3$, green data); the data deviates from the expected zero thermal conductance (solid line). In Fig. 4b we plot λ, for $\Delta N = N_i - N_j = 4 - 2 = 2$, as a function of T_m^2 ($\nu = 2/3$, green data). In both measurements, we find a thermal conductance of $g_Q = (0.33 \pm 0.02)\kappa_0 T$. This value decreased to $g_Q \approx 0.25\kappa_0 T$ when the electron temperature was increased to $T_0 = 30$ mK. With the two edges of each arm being symmetric (a downstream hot mode and an upstream cold mode), the thermal conductance in each edge is

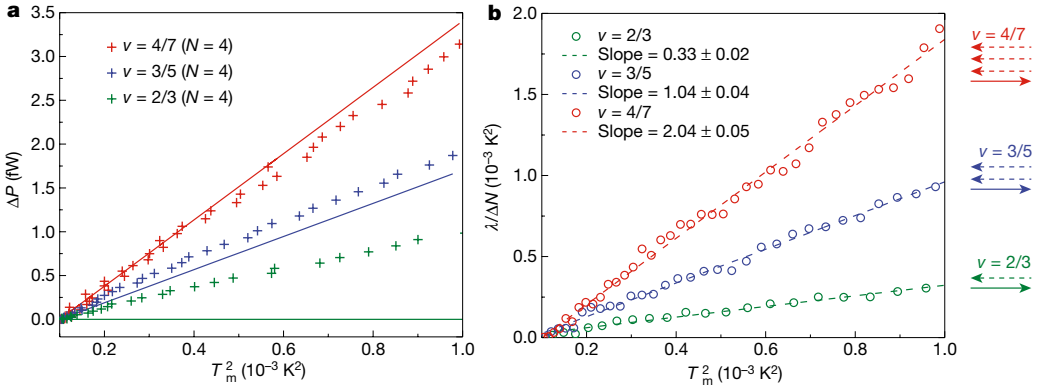

Figure 4 | Measurements of the fractional quantum Hall effect at hole-like states. a, Total power ΔP carried out from the floating contact by the fractional edge modes for $N=4$ in the three hole-like states as function of T_m^2 ($\nu=2/3$, green; $\nu=3/5$, blue; $\nu=4/7$, red). The corresponding expected theoretical results, $\Delta P_e = 0.5 \times 4N_{net}\kappa_0 T_m^2$, with $N_{net}\kappa_0 T$ the expected thermal conductance ($N_{net}=0$ for $\nu=2/3$, $N_{net}=-1$ for $\nu=3/5$ and $N_{net}=-2$ for $\nu=4/7$), are plotted as solid lines; note that, in our device, we see only the absolute value of the thermal conductance. The root-mean-square of the data points deviates from the expected values by 12% for $\nu=3/5$ and by 8.5% for $\nu=4/7$; deviation in the case of $\nu=2/3$ is large (see text). $T_0=10$ mK. **b**, A plot of $\lambda/\Delta N=\delta P/(\kappa_0/2)/\Delta N$, with $\delta P=\Delta P(N_i=4, T_m)-\Delta P(N_j=2, T_m)$, so any phonon contribution is subtracted, as function of T_m^2. The slopes of the linear fits (dashed lines) agree quite well with the predictions for the thermal conductance, except for the $\nu=2/3$ state. Arrows show models of the minimal edge channels for each filling factor: solid arrows depict downstream charged modes and dashed arrows depict upstream neutral modes.

$g_Q \approx (0.17\text{–}0.13)\kappa_0 T$, which is not a large deviation from the expected thermal conductance of zero.

Taking an average arm length of $L \approx 150\,\mu$m, we find that $\xi \approx 30\,\mu$m for $T_0=10$ mK and $\xi \approx 20\,\mu$m for $T_0=30$ mK. These findings are consistent with the increased rate with which energy is exchanged as the base temperature is increased. Interestingly, further increases in the rate of energy exchange lead to a quantization of thermal conductance that improves with increasing temperature. However, non-zero heat flow through the bulk cannot be excluded in this case, owing to the low thermal conductivity of the edges[16].

The state with $\nu_{CF}=3$ or $\nu=3/5$ is expected to have a single net upstream neutral mode ($N_u=2$, $N_d=1$), which carries heat in the limit of long propagation length. Although the total number of modes that are supported by the state is unknown, by gradually pinching a QPC we find two clear lower plateaus at $\nu_{QPC}=2/5$ and $\nu_{QPC}=1/3$, suggesting at least two underlying modes (see Extended Data Fig. 5). Shot noise of the partitioned current in one of these plateaus revealed a quasiparticle charge of $e^*=3e/5$ (see Extended Data Fig. 5), accompanied by upstream neutral modes[13].

We plot the total power dissipation ΔP for $N=4$ in Fig. 4a, and the normalized coefficient λ in Fig. 4b ($\nu=3/5$, blue data). We find an average thermal conductance $g_Q=(1.04\pm0.03)\kappa_0 T$, which agrees very well with our expectations. Increasing the electron temperature to $T_0=30$ mK did not alter the result, presumably owing to the short equilibration length ξ.

In the state with $\nu_{CF}=4$ or $\nu=4/7$, $N_d-N_u=-2$ and the equilibration length is expected to be even shorter (see Methods). Following a similar procedure as described above, we observed three plateaus in a gradually pinched QPC, at $\nu_{QPC}=3/7$, $\nu_{QPC}=2/5$ and $\nu_{QPC}=1/3$, suggesting a larger number of underlying modes (see Extended Data Fig. 5). The partitioned quasiparticle charge (measured in any of these plateaus) was found to be $e^*=4e/7$. We found a nicely quantized thermal conductance of $g_Q=(2.04\pm0.05)\kappa_0 T$ (Fig. 4a, b), reconfirming, again, that the equilibration length is much shorter than the system size ($\xi \ll L$).

To summarize, the extraordinarily precise quantization of the electrical Hall conductance is a good example of a topological phenomenon in physics. Yet, the conductance is just one signature of the topological order, and different orders may exhibit the same conductance. The measurement of topological properties that distinguish between such orders is a key challenge. We address this challenge here by successfully measuring the thermal Hall conductance experimentally. Beyond the obvious difficulties associated with the measurement of thermal Hall conductance, our measurements indicate that the topological protection of this quantization is weaker than that of the electrical Hall conductance; for example, the thermal conductance might depend on the propagation length and on possible heat flow through the bulk.

We verified the value of the quantum of thermal conductance of six different quantum Hall states: two integer states, a particle-like fractional state and three hole-like states. Our results are consistent with the fundamental theory that predicts that fractional modes and chargeless modes carry the same heat as the non-interacting electronic ones (irrespective of their velocities and of the interaction with other chiral modes or the bulk). This type of experiment can be extended to other poorly understood quantum Hall states; for example, there are important questions about the second Landau level, which might host a family of non-Abelian states (such as $\nu=5/2$ and $\nu=12/5$). Some of the proposed topological orders may serve as a platform for universal (topologically based) quantum computations. Thus far, these states have remained enigmatic, with no definitive proof of their nature. Measurements of their thermal conductance would provide compelling evidence of their topological order.

Online Content Methods, along with any additional Extended Data display items and Source Data, are available in the online version of the paper; references unique to these sections appear only in the online paper.

Received 31 October 2016; accepted 3 March 2017.
Published online 17 April 2017.

1. Pendry, J. B. Quantum limits to the flow of information and entropy. *J. Phys. A* **16,** 2161–2171 (1983).
2. Das Sarma, S. & Pinczuk, A. (eds) *Perspectives in Quantum Hall Effects: Novel Quantum Liquids in Low-dimensional Semiconductor Structures* (Wiley, 1996).
3. Schwab, K., Henriksen, E. A., Worlock, J. M. & Roukes, M. L. Measurement of the quantum of thermal conductance. *Nature* **404,** 974–977 (2000).
4. Yung, C. S., Schmidt, D. R. & Cleland, A. N. Thermal conductance and electron–phonon coupling in mechanically suspended nanostructures. *Appl. Phys. Lett.* **81,** 31–33 (2002).
5. Meschke, M., Guichard, W. & Pekola, J. P. Single-mode heat conduction by photons. *Nature* **444,** 187–190 (2006).
6. Molenkamp, L. W., Gravier, Th., van Houten, H., Buijk, O. J. A. & Mabesoone, M. A. A. Peltier coefficient and thermal conductance of a quantum point contact. *Phys. Rev. Lett.* **68,** 3765–3768 (1992).
7. Chiatti, O. *et al.* Quantum thermal conductance of electrons in a one-dimensional wire. *Phys. Rev. Lett.* **97,** 056601 (2006).
8. Jezouin, S. *et al.* Quantum limit of heat flow across a single electronic channel. *Science* **342,** 601–604 (2013).

9. Kane, C. L. & Fisher, M. P. A. Impurity scattering and transport of fractional quantum Hall edge states. *Phys. Rev. B* **51,** 13449–13466 (1995).
10. Kane, C. L. & Fisher, M. P. A. Quantized thermal transport in the fractional quantum Hall effect. *Phys. Rev. B* **55,** 15832–15837 (1997).
11. Cappelli, A., Huerta, M. & Zemba, G. R. Thermal transport in chiral conformal theories and hierarchical quantum Hall states. *Nucl. Phys. B* **636,** 568–582 (2002).
12. Wen, X.-G. *Quantum Field Theory of Many-body Systems: From the Origin of Sound to an Origin of Light and Electrons* (Oxford Univ. Press, 2004).
13. Bid, A. *et al.* Observation of neutral modes in the fractional quantum Hall regime. *Nature* **466,** 585–590 (2010).
14. Gross, Y., Dolev, M., Heiblum, M., Umansky, V. & Mahalu, D. Upstream neutral modes in the fractional quantum Hall effect regime: heat waves or coherent dipoles. *Phys. Rev. Lett.* **108,** 226801 (2012).
15. Gurman, I., Sabo, S., Heiblum, M., Umansky, V. & Mahalu, D. Extracting net current from an upstream neutral mode in the fractional quantum Hall regime. *Nat. Commun.* **3,** 1289 (2012).
16. Inoue, H. *et al.* Proliferation of neutral modes in fractional quantum Hall states. *Nat. Commun.* **5,** 4067 (2014).
17. Wellstood, F. C., Urbina, C. & Clarke, J. Hot-electron effects in metals. *Phys. Rev. B* **49,** 5942–5955 (1994).
18. Jain, J. K. *Composite Fermions* (Cambridge Univ. Press, 2007).
19. Meir, Y. Composite edge states in the $\nu = 2/3$ fractional quantum Hall regime. *Phys. Rev. Lett.* **72,** 2624–2627 (1994).
20. Sabo, R. *et al.* A new paradigm for edge reconstruction in fractional quantum Hall states. *Nat. Phys.* **13,** 4010–4016 (2017).
21. Bid, A., Ofek, N., Heiblum, M., Umansky, V. & Mahalu, D. Shot noise and charge at the 2/3 composite fractional quantum Hall state. *Phys. Rev. Lett.* **103,** 236802 (2009).

Acknowledgements We acknowledge the help and advice of R. Sabo, I. Gurman, N. OfeK, H.-K. Choi and D. Mahalu. M.H. acknowledges the European Research Council under the European Community's Seventh Framework Programme, grant agreement number 339070, the partial support of the Minerva Foundation, grant number 711752, and, together with V.U., the German Israeli Foundation (GIF), grant number I-1241-303.10/2014, and the Israeli Science Foundation (ISF). A.S. and Y.O. acknowledge the European Research Council under the European Community's Seventh Framework Programme (FP7/2007-2013)/ERC, grant agreement number 339070, and the Israeli Science Foundation, ISF agreement number 13335/16. Y.O. acknowledges CRC 183 of the DFG. D.E.F. acknowledges support by the NSF under grant number DMR-1205715.

Author Contributions M.B., A.R. and M.H. designed the experiment. M.B. and A.R. fabricated the devices with input from M.H. A.R. participated in initial measurements. M.B. and M.H. preformed the measurements, did the analysis and guided the experimental work. Y.O., D.E.F. and A.S. worked on the theoretical aspects. V.U. grew the heterostructures in which the two-dimensional electron gas (2DEG) is embedded. All authors contributed to writing the manuscript.

Author Information Reprints and permissions information is available at www.nature.com/reprints. The authors declare no competing financial interests. Readers are welcome to comment on the online version of the paper. Publisher's note: Springer Nature remains neutral with regard to jurisdictional claims in published maps and institutional affiliations. Correspondence and requests for materials should be addressed to M.H. (moty.heiblum@weizmann.ac.il).

Reviewer Information *Nature* thanks G. Gervais and the other anonymous reviewer(s) for their contribution to the peer review of this work.

METHODS

Experimental set-up. An SEM micrograph of the 'heart' of the 4-armed structure is shown in Fig. 1. A floating small contact (light green), playing the part of the floating reservoir, was made in two different sizes: small, about 8 μm^2, in a high-density 2DEG; and large, about 18 μm^2, in a low-density 2DEG. The four arms were formed by chemical etching, each with a main QPC that can be partly or fully pinched. The source contact S is located in arm 1, with two cold pre-amplifiers (cooled to 4.2 K) located in arms 1 and 3 (Extended Data Fig. 1). The amplifier (calibrated by shot-noise measurements) measured the thermal voltage fluctuations S_v after they were filtered by an LC circuit ($f_0 \approx 695$ kHz and bandwidth $\Delta f = 10$–30 kHz, depending on ν). The desired current fluctuations were calculated using $S_{th} = S_v G_H^2$.

Device fabrication. Two different heterojunctions, each hosting a 2DEG, were used: the high-density 2DEG, used in the integer regime, with electron density $n_e = 1.1 \times 10^{11}\,cm^{-2}$, a 4.2-K dark mobility of $\mu = 4 \times 10^6\,cm^2\,V^{-1}\,s^{-1}$, a 2DEG depth below the surface of 113 nm, a spacer to donors of 80 nm and a quantum-well width of 30 nm; and the low-density 2DEG, used in the fractional regime, with $n_e = 0.88 \times 10^{11}\,cm^{-2}$, a 4.2-K dark mobility of $\mu = 4.6 \times 10^6\,cm^2\,V^{-1}\,s^{-1}$, a 2DEG depth below the surface of 128 nm, a spacer to donors of 95 nm and a quantum-well width of 30 nm. Because the electron density tends to decrease near the edge of the contacts[23], a larger floating contact was fabricated in the low-density 2DEG to minimize reflection from the contact. Etched groves under the floating contact (not visible in the SEM micrograph) made sure that the impinging current enters the bulk of the metal ohmic contact before splitting to the different arms.

After a thorough cleaning of the surface (by plasma ashing and oxide removal), contacts were evaporated with an electron-gun evaporator, in a vacuum chamber with a base pressure of 1×10^{-8} torr. The evaporation sequence, from the surface of the GaAs and up, was: Ni (5 nm), Au (200 nm), Ge (100 nm), Ni (75 nm), Au (150 nm). Contacts were alloyed at 450 °C for 50 s.

The TiAu gates of the QPCs were evaporated in the sequence Ti (5 nm), Au (20 nm). Split-gate openings were 700 nm in the high-density 2DEG and 850 nm in the low-density 2DEG. The split gates were shorted by an air bridge made of Ti (20 nm) and Au (480 nm) in a two-layer resist process.

Evaluation of QPCs and contacts. *QPCs.* All of the QPCs were biased at a gate voltage of +0.3 V during the cooling process. This process makes the QPCs more stable and tends to sharpen the confining potential[24,25]. Yet, in the low-density 2DEG and at composite fractions, such as $\nu = 2/5$ and $\nu = 4/3$, the inner edge mode was found to be partly reflected. Even for a zero-bias-cooling process, the QPCs always reflected a sizable part of the impinging current.

Source noise. Some ohmic contacts produced noise at high magnetic field (fillings $\nu < 1/2$), which could be related to a lower density near their periphery[23]. The source noise could be as high as about $1.5 \times 10^{-29}\,A^2Hz^{-1}$ at the highest source current. In such a case (for $\nu = 1/3$), the source noise was divided by 4, 9 or 16, for $N = 2$, 3 or 4, respectively, and subtracted from the measured thermal noise.

Small floating contact. Reflection was measured by comparing the fully reflected current from a pinched QPC (current impinging from the source) and the reflected current for $N = 2$ (or larger). The reflection was always less than 2% in all of the measured fractional states. Assuming this reflection led to shot noise, its magnitude would have been much smaller than the measured thermal noise.

Branching of current to arms. Because the small floating contact might not have the same contact resistance in each of the four arms, equal branching of the impinging current into each arm must be verified. Hence, the transmitted current(s) into the arm(s) of the amplifier(s) was (were) measured when the QPCs in the other arms were either open or fully pinched (see Extended Data Fig. 2).

Calibration of the gain. Knowing the gain of the amplification chain is crucial for determining the electron temperature T_m. Two calibration regions, each one in a different arm, were each composed of an additional QPC and two contacts (see Extended Data Fig. 1). Two methods were used to calibrate the gain: (i) verification of the well-known quasiparticle charge at a known temperature; and (ii) comparison of the gains in different Hall states.

The gain (of the amplification chain, composed of two amplifiers and a spectrum analyser) was calibrated using shot-noise measurements. The temperature is first determined, independent of the gain, by a linear extrapolation of the noise–current curve to zero noise. The intersection point is $eV_H = 2k_BT$, with $V_H = Ivh/e^2$ the Hall voltage (see Extended Data Fig. 5b). With the transmission coefficient of the QPC t_{QPC} and the known quasiparticle charge e^*, the gain is determined by matching the shot-noise data with the expression for the spectral density of the shot noise, $S_I = 2e^*It_{QPC}(1 - t_{QPC})\zeta(V_H, T)$, with $\zeta(x = eV_S/(2k_BT)) = \coth(x) - 1/x$, which has proved to work quite well in all quantum-Hall-effect regimes.

The gain is an 'effective' gain that depends on the bandwidth of the LCR_H circuit. The gain is proportional to the area under the Lorentzian power response of the LCR_H circuit; consequently, the ratio of the areas in different filling factors should be the same as the ratio between the square of the gains (see Extended Data Fig. 5d).

Combining these two methods provides an accurate determination of the gain at each filling factor. It is difficult to determine the systematic errors in the determination of the gain; however, we checked the effects of slightly modifying the gain on the determined temperature T_m, and on the linearity of the data of power dissipation versus T_m^2, and found them to be small in comparison with the natural scattering of the random errors seen in the figures.

Determining T_m. In a general case of multiple one-dimensional edge modes in each of the M arms, the expressions for the dissipated power and the noise are complicated. We express the dissipated power in the floating contact as

$$\Delta P = \frac{1}{2}\frac{I_S^2}{G_0}\frac{\nu_{QPC1}}{\nu^2}\left[1 - \frac{\nu_{QPC1}}{\sum_{i=1}^{4}\nu_{QPCi}}\right]$$

The temperature T_m is related to the thermal noise via $S_{th} = 2G^*k_B(T_m - T_0)$, with

$$\frac{1}{G^*} = \frac{1}{G_{amp}} + \frac{1}{\sum_{i=1, i\neq amp}^{4} G_i}$$

where G_i is the conductance of the ith arm[8,26–29].

Thermal conductance in hole-like states. (See Extended Data Fig. 6.) Here, we discuss heat transport from the floating ohmic contact at the position x_m at temperature T_m and from the grounded contact at position x_0 at a bath temperature T_0. In the Abelian phases of the fractional quantum Hall regime, we expect to have n_d modes emanating from the floating ohmic contact (and moving downstream) and n_u modes emanating from the bath (grounded contacts, moving upstream). In the upper edge, n_u and n_d interchange—n_u modes emanate from the floating ohmic contact and n_d from the bath. For example, for $\nu = 1$ and $\nu = 1/3$, $n_d = 1$ and $n_u = 0$; for $\nu = 2/3$, $n_d = n_u = 1$; and for $\nu = 3/5$, $n_d = 1$ and $n_u = 2$. Henceforth, we discuss the heat flow only at the lower edge of the arms, and add the contribution from the upper edge of the arms at the end of the calculation. To analyse the system, we assume that there is a negligible heat flow through the bulk between the lower and the upper edges. This assumption might not be always valid.

The counter-propagating modes along one edge emanate from two different contacts and are therefore generally at different temperatures. We expect that energy will flow from the hot to the cold modes, owing to their interaction, and denote the energy current between them by $J_t(x)$. Because thermal energy is conserved, we have the following relation between the downstream heat current $J_d(x)$, the upstream heat current $J_u(x)$ and $J_t(x)$:

$$J_d(x + \Delta x/2) = J_d(x - \Delta x/2) - J_t(x)$$
$$J_u(x - \Delta x/2) = J_u(x + \Delta x/2) + J_t(x)$$

Using the one-dimensional relation between the heat current and temperature, $J = KT^2$, with

$$K = \frac{1}{2}\frac{\pi^2k_B^2}{3h}n_{d(u)} = \frac{1}{2}\kappa_0 n_{d(u)}$$

we obtain the differential relations

$$n_d\frac{dT_d^2(x)}{dx} = -j_t(x)$$
$$n_u\frac{dT_u^2(x)}{dx} = -j_t(x) \qquad (1)$$

Here $j_t(x)$ is the heat current density between the downstream and upstream modes (heat exchanged divided by $\kappa_0/2$). In practice, the physical behaviour of $j_t(x)$ can be complex because a few upstream and downstream modes with different energy relaxation rates are in action and the temperature imbalance between them may depend on the position x. However, in a simplified model, we group together all downstream modes and all upstream modes, and adopt Newton's law of cooling, which suggests that

$$j_t(x) = \frac{1}{\xi}[T_d(x)^2 - T_u(x)^2] \qquad (2)$$

This relation is expected to hold for a small temperature difference, and the relaxation length ξ is expected to depend on the average temperature. A solution of equations (1) and (2) (which we describe below), together with the boundary conditions for the lower edge,

$$T_d(x_m) = T_m$$
$$T_u(x_0) = T_0 \qquad (3)$$

provides a full phenomenological description of the heat flow in the system (with n_d and n_u exchanged for the upper edge).

By integrating equations (1) and (2) with respect to x, with the boundary conditions in equation (3), we obtain the temperature of the downstream mode at the lower edge:

$$T_{\mathrm{d}}^{\mathrm{lower}}(x)^2=\frac{T_{\mathrm{m}}^2 n_{\mathrm{d}}\mathrm{e}^{-x_0/(\bar{n}\xi)}+(T_0^2-T_{\mathrm{m}}^2)n_{\mathrm{u}}\mathrm{e}^{-x/(\bar{n}\xi)}-T_0^2 n_{\mathrm{u}}\mathrm{e}^{-x_{\mathrm{m}}/(\bar{n}\xi)}}{n_{\mathrm{d}}\mathrm{e}^{-x_0/(\bar{n}\xi)}-n_{\mathrm{u}}\mathrm{e}^{-x_{\mathrm{m}}/(\bar{n}\xi)}} \quad (4)$$

with $\bar{n}=n_{\mathrm{d}}n_{\mathrm{u}}/(n_{\mathrm{u}}-n_{\mathrm{d}})$. The temperature of the upstream mode at the lower edge is

$$T_{\mathrm{u}}^{\mathrm{lower}}(x)^2=\frac{T_{\mathrm{m}}^2 n_{\mathrm{d}}\mathrm{e}^{-x_0/(\bar{n}\xi)}+(T_0^2-T_{\mathrm{m}}^2)n_{\mathrm{d}}\mathrm{e}^{-x/(\bar{n}\xi)}-T_0^2 n_{\mathrm{u}}\mathrm{e}^{-x_{\mathrm{m}}/(\bar{n}\xi)}}{n_{\mathrm{d}}\mathrm{e}^{-x_0/(\bar{n}\xi)}-n_{\mathrm{u}}\mathrm{e}^{-x_{\mathrm{m}}/(\bar{n}\xi)}} \quad (5)$$

To determine the temperature profile of the modes in the upper edge, we interchange n_{d} and n_{u}. The normalized two-terminal thermal conductance coefficient (which is unity in case of $\nu=1$) is positive by definition and is composed of two parts, corresponding to the heat flow along the upper and lower edges. The contribution of the lower edge is

$$K_{\mathrm{lower}}=\frac{J_{\mathrm{d}}(x)-J_{\mathrm{u}}(x)-J_{\mathrm{p}}}{0.5\kappa_0(T_{\mathrm{m}}^2-T_0^2)}=\frac{n_{\mathrm{d}}T_{\mathrm{d}}^{\mathrm{lower}}(x)^2-n_{\mathrm{u}}T_{\mathrm{u}}^{\mathrm{lower}}(x)^2-(n_{\mathrm{d}}-n_{\mathrm{u}})T_0^2}{T_{\mathrm{m}}^2-T_0^2} \quad (6)$$

Here, $J_{\mathrm{p}}=0.5\kappa_0(n_{\mathrm{d}}-n_{\mathrm{u}})T_0^2$ is the persistent heat flow in the system at equilibrium, which is a consequence of the edge being chiral. This heat flow is transverse and has no divergence, because the upper edge has an opposite term. We subtract it from both edges, because we are interested in the excess thermal noise. Substituting equations (4) and (5) into equation (6) (notice that the space-dependent terms in the numerators cancel out) we obtain

$$K_{\mathrm{lower}}=\frac{n_{\mathrm{d}}(n_{\mathrm{d}}-n_{\mathrm{u}})}{n_{\mathrm{d}}-n_{\mathrm{u}}\mathrm{e}^{L/(\bar{n}\xi)}} \quad (7)$$

where $L=x_0-x_{\mathrm{m}}$. To obtain K_{upper} we interchange n_{u} and n_{d} (also in the expression for $\bar{n}$), which yields

$$K_{\mathrm{upper}}=\frac{n_{\mathrm{u}}(n_{\mathrm{u}}-n_{\mathrm{d}})}{n_{\mathrm{u}}-n_{\mathrm{d}}\mathrm{e}^{-L/(\bar{n}\xi)}} \quad (8)$$

In the experiment, heat is flowing out of the floating contact from both of its sides, the lower and the upper edges of each arm, so that we actually measure the sum of them:

$$K\equiv K_{\mathrm{lower}}+K_{\mathrm{upper}}=(n_{\mathrm{d}}-n_{\mathrm{u}})\left[\frac{2n_{\mathrm{d}}}{n_{\mathrm{d}}-n_{\mathrm{u}}\mathrm{e}^{L/(\bar{n}\xi)}}-1\right] \quad (9)$$

Using the general expressions given in equations (4), (5) and (7)–(9), we reach several conclusions about the structure of the temperature profile and the thermal conductance in the fractional quantum Hall states.

$\nu=1$ and $\nu=1/3$. In these cases, $n_{\mathrm{d}}=1$ and $n_{\mathrm{u}}=0$. An application of equation (4) gives $T_{\mathrm{d}}^{\mathrm{lower}}(x)=T_{\mathrm{m}}$ and $T_{\mathrm{u}}^{\mathrm{upper}}(x)=T_0$, which are independent of x. Moreover, with $\bar{n}=0$, equations (7)–(9) give $K_{\mathrm{lower}}=1$, $K_{\mathrm{upper}}=0$ and $K=1$, so that, as expected, the heat is carried out of the floating contact by the downstream mode via the lower edge.

$\nu=2/3$. In this case, $n_{\mathrm{u}}=n_{\mathrm{d}}=1$. However, formally $\bar{n}\to\infty$ as $n_{\mathrm{d}}\to n_{\mathrm{u}}$, so we have to take this limit carefully. Doing so, we obtain

$$T_{\mathrm{d}}^2(x)=\frac{T_{\mathrm{m}}^2[L/\xi-(x-x_{\mathrm{m}})/\xi]+T_0^2[(x-x_{\mathrm{m}})/\xi]+T_{\mathrm{m}}^2}{1+L/\xi}$$

$$T_{\mathrm{u}}^2(x)=\frac{T_{\mathrm{m}}^2[L/\xi-(x-x_{\mathrm{m}})/\xi]+T_0^2[(x-x_{\mathrm{m}})/\xi]+T_0^2}{1+L/\xi}$$

In this case, the temperature depends linearly on x, but the difference between the temperatures of the upstream and downstream modes is constant:

$$T_{\mathrm{d}}^2(x)-T_{\mathrm{u}}^2(x)=\frac{T_{\mathrm{m}}^2-T_0^2}{1+L/\xi}$$

The upstream and downstream modes fully equilibrates only for $L\gg\xi$, in which case

$$K_{\mathrm{lower}}=K_{\mathrm{upper}}=\frac{1}{1+L/\xi}$$

$$K=\frac{2}{1+L/\xi}$$

For $\xi\gg L$, the upstream and downstream modes do not fully equilibrate and two modes (the charge mode at the lower edge and the neutral mode at the upper edge) conduct heat. When $\xi\ll L$, the system does not conduct electronic heat. The interpolation between the two extremes is algebraic.

In our experiment, K was measured for two bath temperatures: for $T_0=10\,\mathrm{mK}$ we measure a normalized thermal conductance $K\approx0.33$ (and not zero); and for $T_0=30\,\mathrm{mK}$ we find $K\approx0.25$. Counter-intuitively, the quantization increases as the temperature increases. This is explained by the improved equilibration at high temperature. Taking and average arm length of $L\approx150\,\mu\mathrm{m}$, we find $\xi\approx30\,\mu\mathrm{m}$ for $T_0=10\,\mathrm{mK}$ and $\xi\approx20\,\mu\mathrm{m}$ for $T_0=30\,\mathrm{mK}$. Note that, because the sample has several arms of different length L, the estimates of the relaxation lengths are approximate.

$\nu=3/5$ and $\nu=4/7$. For the case $\nu=3/5$, $n_{\mathrm{u}}=2$ and $n_{\mathrm{d}}=1$. According to equations (4) and (5), the temperatures of the downstream and upstream modes equilibrate after a length $\bar{n}\xi$, with $\bar{n}=n_{\mathrm{d}}n_{\mathrm{u}}/(n_{\mathrm{u}}-n_{\mathrm{d}})=2$.

On the lower edge, the temperature of the single downstream mode (which emanates from the hot floating contact at temperature T_{m}) is reduced exponentially the temperature of the two upstream modes (which emanate from the cold bath at temperature T_0). On the upper edge, the situation is reversed: the temperature of all of the modes in the upper edge is equal to T_{m} at x_{m}, and starts to decrease only at a distance $\bar{n}\xi$ away from the cold bath. There, the temperature of the downstream mode approaches T_0, and that of the two upstream modes is reduced from T_{m} to a lower value.

In the limit $L\gg\xi$, we find normalized values $K_{\mathrm{lower}}=0$ and $K_{\mathrm{upper}}=1$, with small exponential corrections. The heat is conducted by the modes on the upper edge and the measurements show quantization of the thermal conductance with high accuracy. Taking $L/(2\xi)=3$, similar to the low-temperature value for $\nu=2/3$, we obtain a correction of about 0.05, which is similar to our experimental accuracy.

For $\nu=4/7$, $n_{\mathrm{u}}=3$ and $n_{\mathrm{d}}=1$; hence, $\bar{n}=3/2$. In this case we expect an even better quantization of the thermal conductance. This is consistent with the experimental observations.

Edge reconstruction. When the confining potential at the edge is smooth enough, edge reconstruction may introduce additional achiral modes. Crudely, these may be thought of as leading to an equal increase in both n_{u} and n_{d}, and hence to a larger $\bar{n}$ and longer relaxation length.

An interesting experimental fact. The hole-like states appeared to be 'experimentally friendly' in these experiments. Their conductance plateaus in the transmission of the QPCs lend themselves to a constant conductance in the nonlinear regime (independent of the current in the measurement regime). In particular, the dip in the density of the electrons, that may take place near the periphery of the contacts, does not seem to lead to any reflection and excess noise (as we find in the integer regime or in the particle-like states). We attribute this effect to an increase in the composite-fermion filling as the density decreases (as the fillings approach $\nu=1/2$), enabling a smooth traversal of the edge modes of lower composite-fermion filling fractions[18].

Data availability. The datasets generated and analysed during this study are available from the corresponding author on reasonable request.

22. Slobodeniuk, A. O., Levkivskyi, I. P. & Sukhorukov, E. V. Equilibration of quantum Hall edge states by an Ohmic contact. *Phys. Rev. B* **88,** 165307 (2013).
23. Dahlem, F. Cryogenic scanning force microscopy of quantum Hall samples: adiabatic transport originating in anisotropic depletion at contact interfaces. *Phys. Rev. B* **82,** 121305 (2010).
24. Buks, E., Heiblum, M., Levinson, Y. & Shtrikman, H. Scattering of a two-dimensional electron gas by a correlated system of ionized donors. *Semicond. Sci. Technol.* **9,** 2031–2041 (1994).
25. Buks, E., Heiblum, M. & Shtrikman, H. Correlated charged donors and strong mobility enhancement in a two-dimensional electron gas. *Phys. Rev. B* **49,** 14790(R)–14793(R) (1994).
26. Sivan, U. & Imry, Y. Multichannel Landauer formula for thermoelectric transport with application to thermopower near the mobility edge. *Phys. Rev. B* **33,** 551–558 (1986).
27. Jiang, J.-H. & Imry, Y. Linear and nonlinear mesoscopic thermoelectric transport with coupling to heat bath. *C. R. Phys.* **17,** 1047–1059 (2016).
28. Beenakker, C. W. J. & Buttiker, M. Suppression of shot noise in metallic diffusive conductors. *Phys. Rev. B* **46,** 1889–1892 (1992).
29. Blanter, Y. M. & Sukhorukov, E. V. Semiclassical theory of conductance and noise in open chaotic cavities. *Phys. Rev. Lett.* **84,** 1280–1283 (2000).

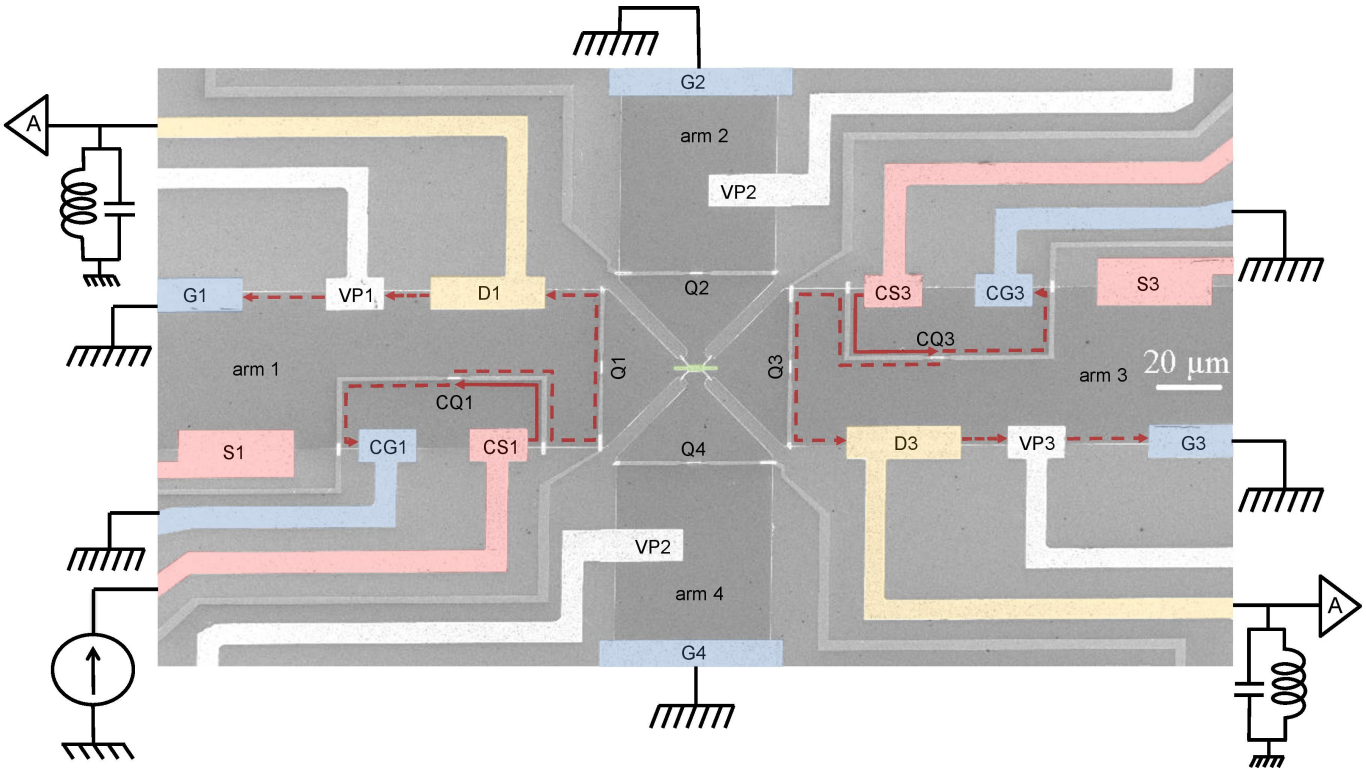

Extended Data Figure 1 | Detailed schematic of the structure. The SEM micrograph shows details away from the floating ohmic contact. In particular, note the two calibration regions, each hosting an added source contact (CS1 or CS3), a ground contact (CG1 or CG3) and a QPC (CQ1 or CQ3, which is fully pinched when thermal noise is measured). When QPC1 is fully pinched and CQ1 is partly pinched, shot noise is measured by the amplifier at D1 (in the same arm), with respect to ground. There are also voltage probes (VP) in each arm for low-frequency lock-in measurements. Q1–Q4 denote QPC1–QPC4.

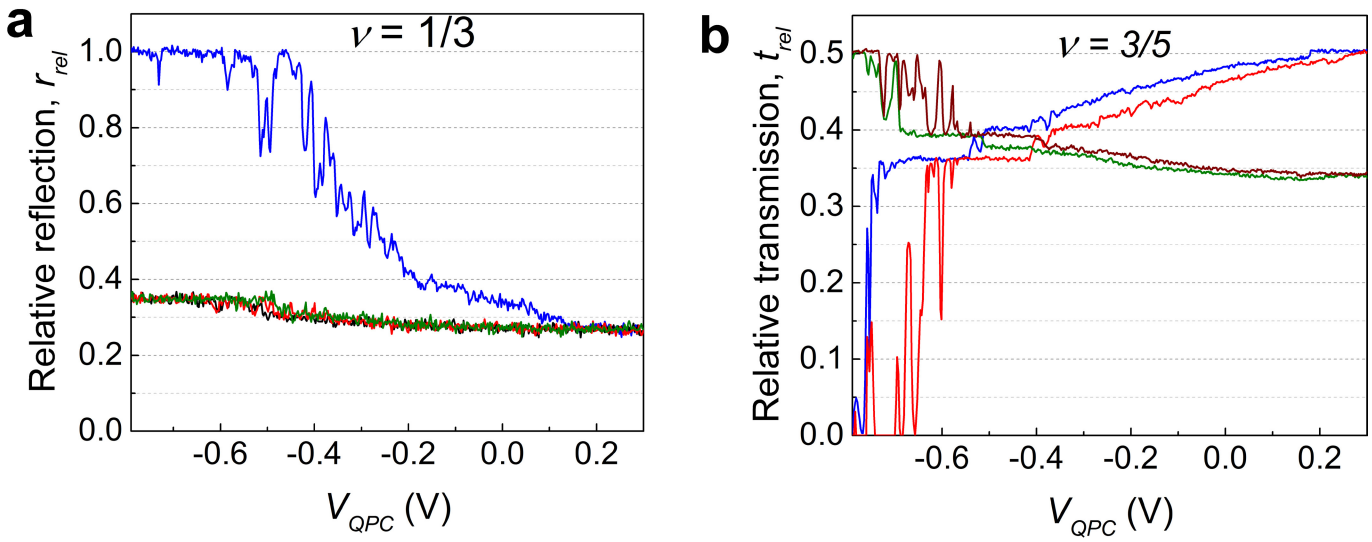

Extended Data Figure 2 | Current splitting among multiple arms. **a**, $\nu = 1/3$. Current is sourced from S and measured by the amplifier at D1 (see notations in Fig. 1). The blue curve is the reflection coefficient r_{rel} into D1 (a function of the pinching of QPC1) when all of the QPCs in the other arms are open. The other lines correspond to when the QPC in each of the arms pinches separately, while QPC1 is fully open. We see that each arm consumes the same current. V_{QPC} represents the pinching of the relevant QPC. **b**, $\nu = 3/5$. A similar experiment as for **a**, but in this case the current is sourced from S and measured at D3 as each of the other QPCs pinch. The red and blue lines are the transmissions of QPC1 and QPC3 while both QPC2 and QPC4 were completely pinched; hence, the relative transmission starts from $t_{rel} = 0.5$ and goes down to zero. The other two lines are the transmissions of QPC2 while all QPCs except QPC4 were open, and of QPC4 while all QPCs except QPC2 were open. In these cases, the relative transmission starts from 0.33 and reaches 0.5 when QPC2 or QPC4 was completely pinched.

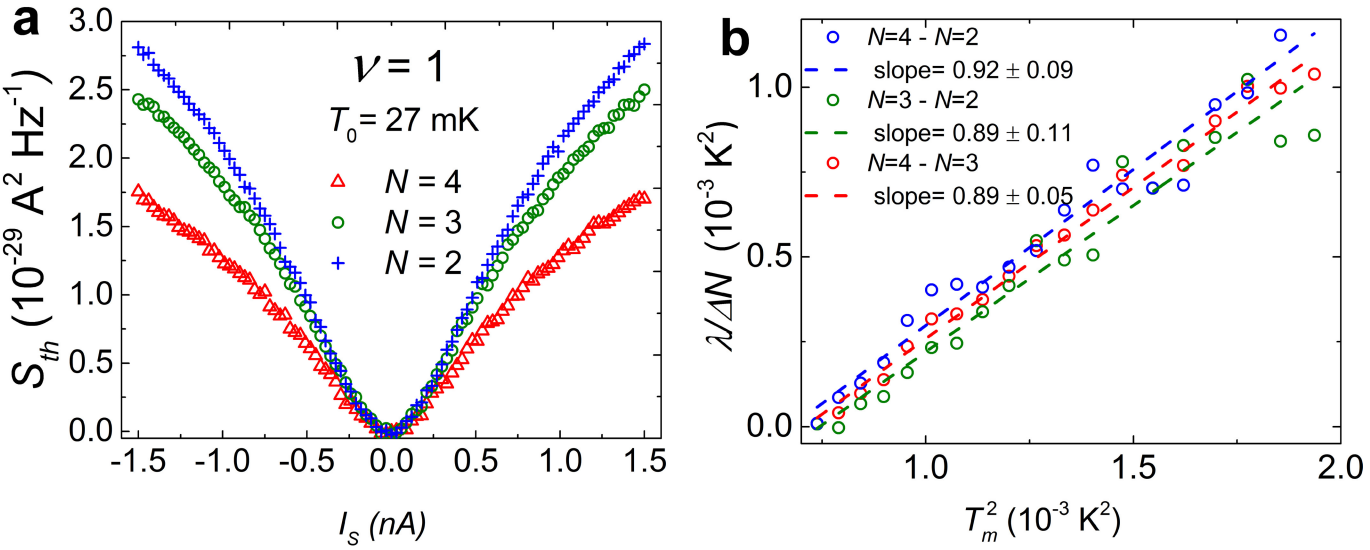

Extended Data Figure 3 | Thermal noise and analysis at $\nu = 1$. **a**, Thermal noise S_{th} as a function of $I_S = I_{in}$ for different numbers of arms (N). **b**, The normalized subtracted power dissipation λ (see main text) as function of T_m^2 ($T_m < 40$ mK). Subtracting the contributions for different N cancels out the phonon contribution; the notation in the legend, for example, '$N = 4 - N = 2$', indicates the power dissipation for four arms, less that for two arms. The fit lines lead to an average thermal conductance per channel of $g_Q = (0.9 \pm 0.1)\kappa_0 T$.

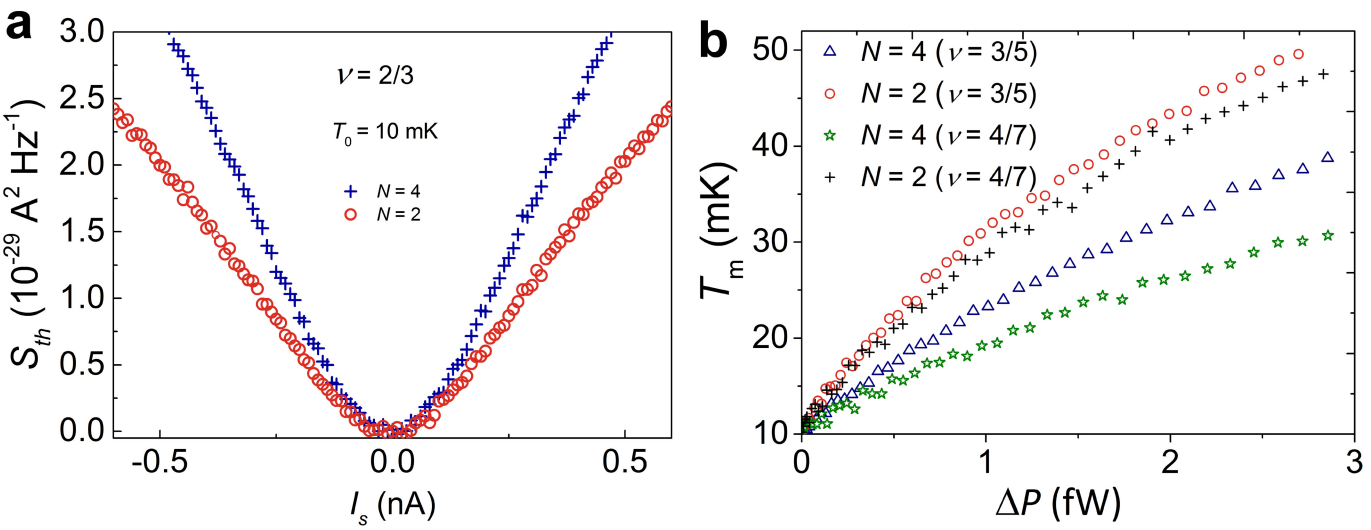

Extended Data Figure 4 | Raw data of thermal noise S_{th} and T_m for hole-like states. a, Thermal noise S_{th} for two different arm configurations and $\nu = 2/3$, as a function of source current I_S. **b**, Deduced T_m as function of the dissipated power ΔP in the floating ohmic contact for the two arm configurations and $\nu = 3/5$ or $\nu = 4/7$ ($T_0 = 10$ mK).

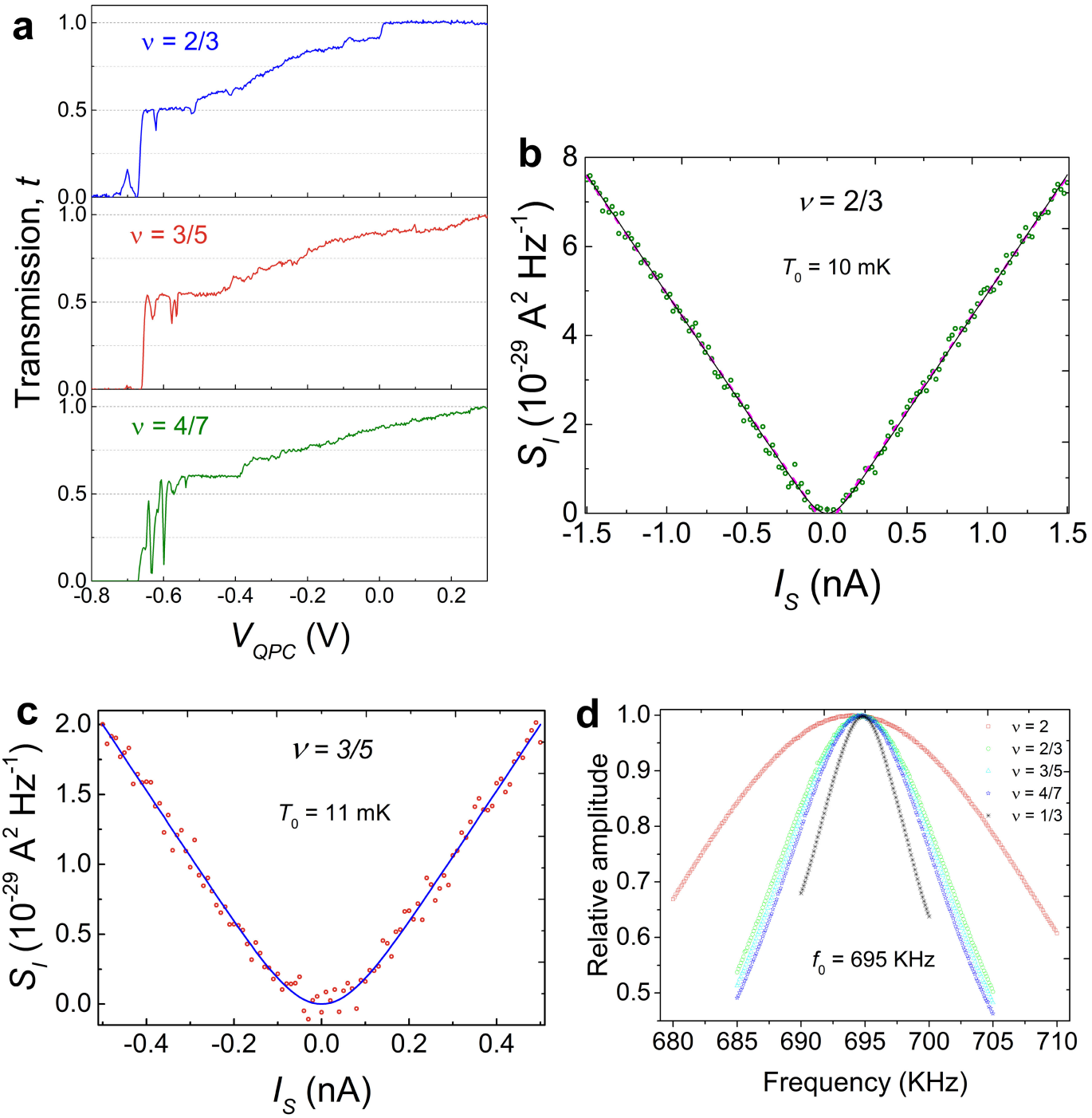

Extended Data Figure 5 | Gain and temperature calibration via shot noise. a, Transmission t of a QPC for $\nu = 2/3$ (blue, top), $\nu = 3/5$ (red, middle) and $\nu = 4/7$ (green, bottom). Plateaus are visible for the different chiral charge modes at the edge. **b**, Shot noise S_I (green circles) measured for $\nu = 2/3$ at the $t = 0.5$ plateau to calibrate the gain. The black solid line shows a fit with the equation $2e^*I_S t(1-t)\coth[e^*V_S/(2k_BT_0)] - 2k_BT_0/(e^*V_S)]$, with $e^* = 2e/3$ and $T_0 = 10$ mK. Linear extrapolation of this fit to zero noise from $V_S = (e^2/h)I_S = 2k_BT_0$ (dashed magenta line) provides an exact measure of T_0 that is independent of the gain. **c**, Shot noise S_I (red circles) measured for $\nu = 3/5$ at the $t = 0.55$ plateau, with the blue solid line corresponding to a fit using the expression in **b**, but with $e^* = 3e/5$ and $T = 11$ mK. **d**, Resonant response of the LCR_H circuit (connected to the drain in parallel with the actual device) at different filling factors. Gains at different filling factors are compared by the ratio of the areas in the appropriate bandwidths. At smaller filling factors, the bandwidth is smaller (largest 30 kHz, smallest 10 kHz).

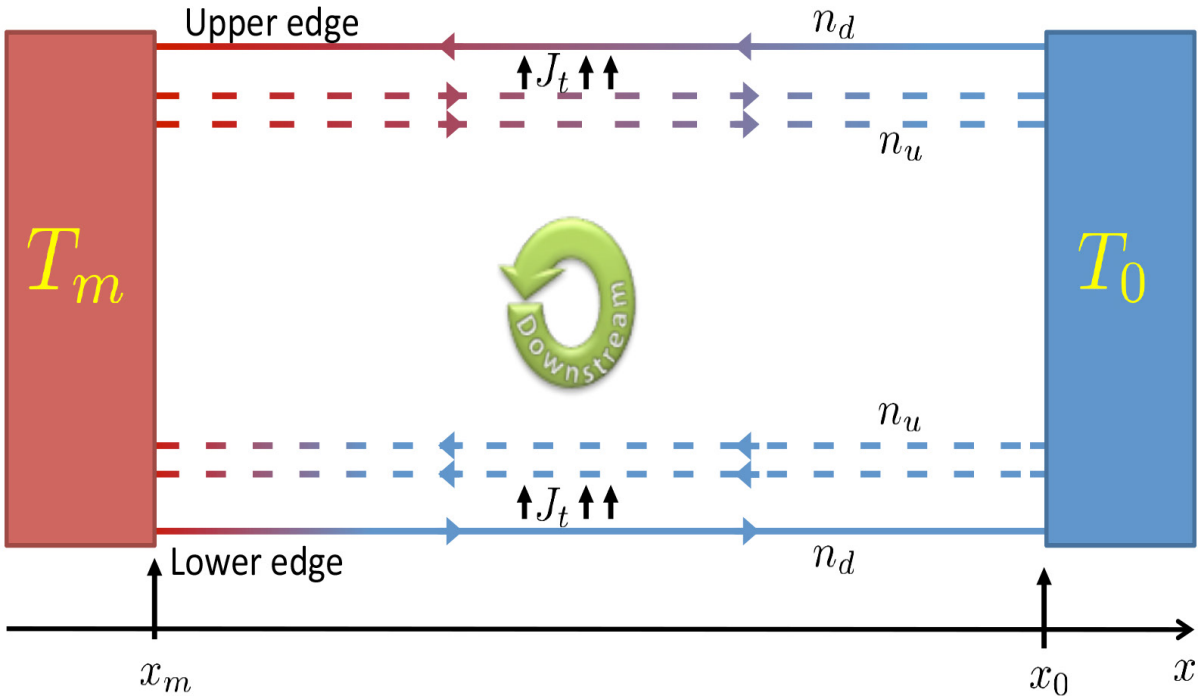

Extended Data Figure 6 | Schematics aiding the calculation of the equilibration length in Methods (and the main text). The schematic shows a single arm with n_d downstream modes (in the chiral direction; solid arrows) and n_u upstream modes (in the achiral direction; dashed arrows). The arrows marked as J_t represent energy exchange in the equilibration process. The relevant length of each arm is $L = x_0 - x_m$.